

Josephson junction-based axion detection through resonant activation

Roberto Grimaudo,¹ Davide Valenti,¹ Bernardo Spagnolo,^{1,2} Giovanni Filatrella,^{3,4} and Claudio Guarcello^{5,4}

¹*Dipartimento di Fisica e Chimica “E. Segrè”, Università degli Studi di Palermo,
Viale delle Scienze Ed. 18, I-90128 Palermo, Italy*

²*Lobachevskii University of Nizhni Novgorod, 23 Gagarin Ave. Nizhni Novgorod 603950 Russia*

³*Dep. of Sciences and Technologies, University of Sannio, Via De Sanctis, Benevento I-82100, Italy*

⁴*INFN, Sezione di Napoli Gruppo Collegato di Salerno,
Complesso Universitario di Monte S. Angelo, I-80126 Napoli, Italy*

⁵*Dipartimento di Fisica “E.R. Caianiello”, Università di Salerno,
Via Giovanni Paolo II, 132, I-84084 Fisciano (SA), Italy*

(Dated: April 15, 2022)

We discuss the resonant activation phenomenon on a Josephson junction due to the coupling of the Josephson system with axions. We show how such an effect can be exploited for axion detection. A nonmonotonic behavior, with a minimum, of the mean switching time from the superconducting to the resistive state versus the ratio of the axion energy and the Josephson plasma energy is found. We demonstrate how variations in switching times make it possible to detect the presence of the axion field. An experimental protocol for observing axions through their coupling with a Josephson system is proposed.

I. INTRODUCTION

Very recently the dark-matter axion detection has become a promising and fruitful research field [1–14]. Josephson systems are recognized of paramount importance as a sensitive experimental tool, as a playground for many theoretical models, and for their applications in fast, low-noise electronics [15–27]. In the last years, a Josephson junction (JJ) has been supposed to interact with axions, the hypothetical elementary particles proposed as a possible component of cold dark matter [28–30], by exploiting the matching between the energies of the axion and the JJ [31–33]. Very recently, hard X-ray emission from neutron stars has been explained by axion emission [34, 35]. The axion’s mass estimation is compatible with the values postulated by the Peccei-Quinn theory introduced in 1977 to solve the strong CP problem in quantum chromodynamics [36]. The theory introduces a new scalar field which spontaneously breaks the symmetry at low energies, giving rise to an axion that suppresses the CP violation [37, 38]. Moreover, unexplained events in Josephson-based experiments [39–43] can be well justified on the basis of the axion-JJ coupling. This hypothesis has thus paved the way to think of JJs as possible axion-detectors. However, up to now, no systematic investigations of resonance experimental conditions, suitable for direct Josephson-based axion detection, have been carried out.

Here, we consider a Josephson-based detector to exploit the measurable voltage drop that appears across the device when the combined action of bias current and thermal fluctuations induces the switch from the superconducting to the resistive state [27, 44–46]. In the presence of axion coupling, the analysis of the mean switching times (MST), τ_{MST} , for the JJ reveals the occurrence of a resonance effect. This is the axion-induced resonant activation phenomenon characterized by a nonmonotonic be-

havior of τ_{MST} , with a minimum, versus the ratio of the axion to the Josephson plasma energy. Furthermore, our work allows the identification of the suitable experimental conditions for a Josephson system to effectively detect such an axion-JJ resonance. Based on these findings, an experimental procedure for observing axions coupled to a JJ system is proposed.

The paper is organized as follows. The physical characteristics and the mathematical formalism of the two subsystems, JJ and axion, and the composed axion-JJ system are presented in Secs. II, III and IV, respectively. In Sec. V, the axion-induced resonant activation phenomenon is discussed in detail, while in Sec. VI the outlines of two possible experimental schemes are proposed. Finally, conclusive remarks are reported in Sec. VII.

II. RCSJ MODEL

We consider a superconductor-normal metal-superconductor JJ (see Appendix A 1), Fig. 1(a), whose phase dynamics can be described within the resistively and capacitively shunted junction (RCSJ) model [15, 27, 47, 48] as

$$\beta_C \frac{d^2\varphi(\tau_c)}{d\tau_c^2} + \frac{d\varphi(\tau_c)}{d\tau_c} + \sin[\varphi(\tau_c)] = i_n(\tau_c) + i_b. \quad (1)$$

The time is normalized to the inverse of the characteristic frequency, that is $\tau_c = \omega_c t$ with $\omega_c = (2e/\hbar) I_c R$. I_c is the maximum Josephson current that can flow through the device, while $i_b = I_b/I_c$ and $i_n = I_n/I_c$ are, respectively, the normalized external bias current and thermal noise current. $\beta_C = \omega_c RC$ is the Stewart-McCumber parameter, with R and C being the normal-state resistance and capacitance of the JJ, respectively. A JJ can be effectively described in terms of a particle moving along a washboard potential tilted by i_b (see Appendix A 1),

see Fig. 1(b). Increasing i_b , the slope of the washboard potential increases and the height of the confining potential barrier reduces, up to vanish altogether for $i_b = 1$. Overdamped and underdamped JJs are characterized by $\beta_c \ll 1$ and $\beta_c \gg 1$, respectively.

In this work, the random current is modeled as a standard Gaussian white noise associated to the JJ resistance, with the usual statistical properties $\langle i_n(\tau) \rangle = 0$ and $\langle i_n(\tau) i_n(\tau + \tilde{\tau}) \rangle = 2D \delta(\tilde{\tau})$. The amplitude of the normalized correlation is connected with the physical temperature T through the relation [15]

$$D = \frac{k_B T \omega_c}{R I_c^2}. \quad (2)$$

III. AXION FIELD

An axion field a is characterized by two parameters, the axion misalignment angle θ and the axion coupling constant f_a , namely $a = f_a \theta$ [49]. Within the Robertson-Walker metric, which is appropriate to describe the early universe, the homogeneous equation of motion of the axion misalignment angle θ reads [37]

$$\frac{d^2\theta(t)}{dt^2} + 3H \frac{d\theta(t)}{dt} + \frac{m_a^2 c^4}{\hbar^2} \sin[\theta(t)] = 0. \quad (3)$$

Here, $H \approx 2 \times 10^{-18} \text{ s}^{-1}$ is the Hubble parameter and m_a denotes the axion mass.

It is evident the similarity between the equations of motion governing the axion and the RCSJ systems: the axion dynamics is analogous to that of a RCSJ with no externally applied bias current. Besides the formal mathematical analogy between the two systems, it is physically remarkable that the parameters characterizing the two equations are quite similar as their order of magnitude is concerned (see Appendix A 2).

IV. AXION-JJ SYSTEM

The interaction between axion and JJ can be formally written as

$$\ddot{\varphi} + a_1 \dot{\varphi} + b_1 \sin(\varphi) = \gamma(\ddot{\theta} - \ddot{\varphi}), \quad (4a)$$

$$\ddot{\theta} + a_2 \dot{\theta} + b_2 \sin(\theta) = \gamma(\ddot{\varphi} - \ddot{\theta}), \quad (4b)$$

where (a_1, a_2) and (b_1, b_2) are the dissipation and frequency parameters, respectively; γ is the coupling constant between axion and JJ and its value can be inferred from experimental quantities [33]. In analogy to what happens in resonant cavities, the axion-JJ coupling is supposed to be responsible for the decay of the axion into two photons, one of which (that characterized by a vanishing moment) generates electron-hole pairs which in turn create a supercurrent [28–31].

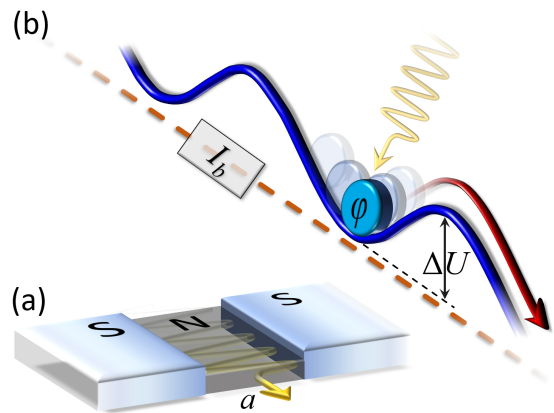


FIG. 1. (a) Schematic illustration of the device. An axion field a through the weak link is also represented. (b) Phase particle in a minimum of the washboard potential U , tilted by a bias current. The phase can overcome the potential barrier, ΔU , rolling down along the potential because of the combined effect of thermal noise and axion-JJ coupling.

By considering the presence of both a bias current and thermal fluctuations in the JJ equation, the axion-JJ system [Eqs. (4)] can be conveniently rewritten as (see Appendix B)

$$\frac{\beta_c}{k_2} \ddot{\varphi} + \dot{\varphi} + \sin(\varphi) + \frac{k_1}{k_2} \varepsilon \sin(\theta) = i_b + i_n, \quad (5a)$$

$$\frac{\beta_c}{k_1} \ddot{\theta} + \dot{\theta} + \sin(\theta) + \frac{k_2}{k_1} \varepsilon \sin(\varphi) = i_b + i_n, \quad (5b)$$

with

$$k_1 = \frac{\gamma}{1 + 2\gamma}, k_2 = \frac{1 + \gamma}{1 + 2\gamma}, \beta_c = \frac{\omega_c^2}{\omega_p^2}, \varepsilon = \left(\frac{m_a c^2}{\hbar \omega_p} \right)^2, \quad (6)$$

where $\omega_p = \sqrt{(2eI_c)/(\hbar C)}$ is the Josephson plasma frequency. We assume that the additional sinusoidal term depending on θ in Eq. (5a) can be ascribed to the Cooper-pair current indirectly induced by the axion entering the junction. In other words, the axion induces an extra current term. The ε parameter indicates the ratio between the axion energy and the Josephson plasma energy, $\hbar \omega_p$, and represents our “control knob” to set the most convenient working point for the detection of an axion field interacting with the JJ. Indeed, the Josephson plasma frequency, and therefore the energy ratio ε , can be “adjusted” as needed, since I_c can be lowered by raising the temperature [50], applying a magnetic field [51] or a gate voltage [52, 53]. In this way, the system response can be tuned to achieve a working regime in which the switching dynamics of the axion-JJ coupled system well deviates from the Josephson response in the absence of axions. This condition makes the axion-JJ interaction clearly detectable.

Now we analyze how the axion affects the MST, i.e. the average time the JJ system takes to switch from the initial superconducting state (particle at the bottom of

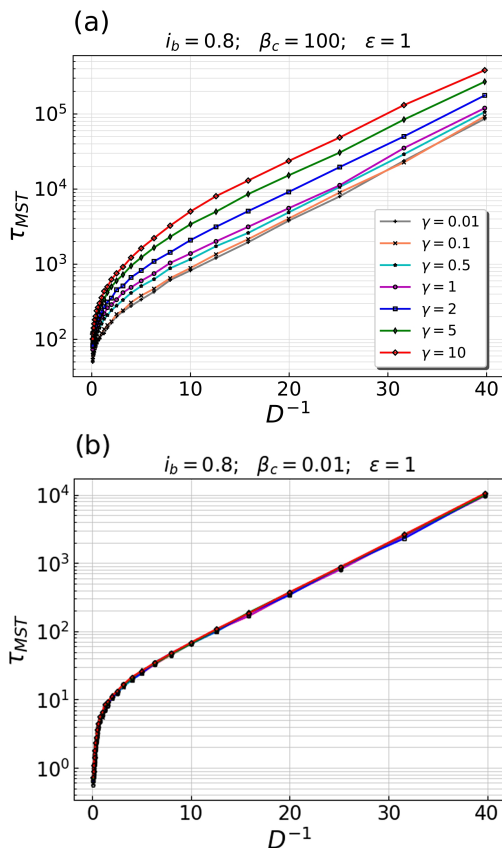


FIG. 2. Semilog plot of the mean switching time (τ_{MST}) versus the inverse noise intensity (D^{-1}), in the under- [(a)] and over- [(b)] damped regime for a JJ, that is the coupling and decoupling regime, respectively, in the presence of thermal noise and an external bias current $i_b = 0.8$, at different values of γ . The legend in (a) refers to both panels.

the well) to the resistive state. Due to random thermal fluctuations, the particle can escape from the potential well, even if the junction is biased by a current below the critical value (i.e., $i_b < 1$). According to Kramers' theory, in the strong damping limit the average escape rate from a neighbouring potential barrier $\Delta U(i_b)$ in the presence of a noise source, with intensity D expressed by Eq. (2), is given in the simplest approximation by the following expression [47]

$$r(i_b, D) = \frac{\omega_c}{2\pi} (1 - i_b^2)^{\frac{1}{4}} e^{-\frac{\Delta U(i_b)}{D}}. \quad (7)$$

In Fig. 2 we show the behavior of the normalized MST, τ_{MST} , as a function of the inverse of the noise intensity, D^{-1} , under different damping conditions, performing $N = 10^4$ independent numerical realizations from Eqs. (5). The linear behavior of τ_{MST} vs D^{-1} characterizes a Kramers-like law. We note that if we multiply Eq. (4a) by β_c , the latter appears only in the second-derivative terms, while the first-derivative term will be multiplied by the square root of β_c . Consequently, under the overdamped approximation ($\beta_c \ll 1$)

the coupling term $\beta_c \gamma (\ddot{\theta} - \ddot{\varphi})$ becomes negligible with respect to all the other terms in Eq. (4a) and the two equations decouple, as it is evident by comparing the two panels in Fig. 2. Therefore, a suitable regime for the JJ system to detect axions is the underdamped regime ($\beta_c \gg 1$).

Furthermore, the axion-coupling induces only a shift of the τ_{MST} curves upwards as the coupling parameter increases, while the slope is substantially unchanged (Fig. 2). Therefore, only the prefactor of the Kramers-like law is influenced by γ and not the height of the effective potential barrier [54, 55], which is given by the slope of the curves of Fig. 2(a).

V. RESONANT ACTIVATION EFFECT

In light of the above result, it is interesting to study the dependence of the MST on the ratio ε between the axion energy and the Josephson plasma energy. We further emphasize that the Josephson energy depends on the plasma frequency ω_p and, therefore, it can be tuned in experiments. However, the energy cannot be lowered at will, for example it is always necessary to ensure that the intensity of the thermal fluctuations is much lower than the critical current of the junction.

Figure 3(a) clearly shows a significant nonmonotonic behavior of τ_{MST} vs ε , with a minimum in the range $\varepsilon \in [0.1, 1]$, which is a signature of an axion-JJ resonant activation phenomenon, observed in JJs both in the absence and presence of a noise source [16, 18, 56]. This resonant phenomenon is ascribed to the frequency-matching condition between the frequency associated to the axion angle field θ and the JJ plasma frequency (see Appendix B). In fact, the term $(k_1/k_2)\varepsilon \sin(\theta)$ in Eq. (5a) can be interpreted as an oscillating current for the Josephson system, which is responsible for the resonant activation phenomenon [16, 18]. The minimum is less pronounced for low and high values of γ . In particular, for low values of the coupling parameter, $\gamma \lesssim 0.5$, the minimum is affected by the decoupling, which smoothes the curve towards a constant behavior; for high coupling values, $\gamma \gg 0.5$, very high values of τ_{MST} , due to the confinement of the JJ phase particle ($\varepsilon \gtrsim 1$), tend to shallow the minimum. In the intermediate range, the minimum is more pronounced showing the resonant activation phenomenon. Indeed, by linearizing Eqs. (4), in the absence of noise, we get in the underdamped regime the expression for the frequency associated with the axion-JJ system (see Appendix B)

$$\omega_p^+(\gamma, \varepsilon) = \omega_p \sqrt{\frac{k_2(\varepsilon + 1) + f(\gamma, \varepsilon)}{2}}, \quad (8)$$

with

$$f(\gamma, \varepsilon) = \sqrt{k_2^2(\varepsilon - 1)^2 + 4k_1^2\varepsilon}. \quad (9)$$

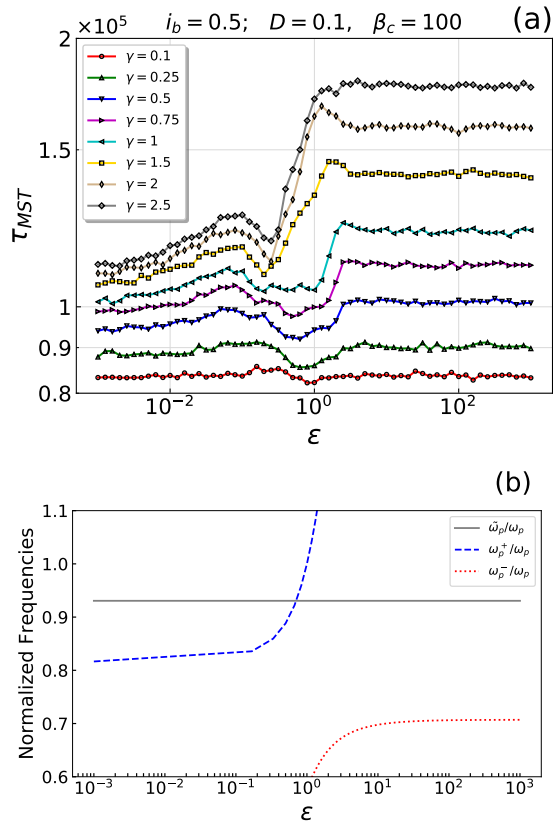


FIG. 3. (a) Log-log plot of the dependence of the mean switching time (τ_{MST}) on the energy ratio ϵ , in underdamped regime ($\beta_c = 100$), with $i_b = 0.5$ and $D = 0.1$ for a JJ subject to thermal noise and coupled with an axion field. The statistics is based on a set of $5 \cdot 10^4$ realizations. (b) Semilog plot of two normalized frequencies ω_p^+ (dashed blue line) and ω_p^- (dotted red line), which characterize the axion-JJ dynamics in the underdamped ($\beta_c = 100$) small-oscillation ($\dot{\varphi} \rightarrow 0$) regime with $\gamma = 1.0$, vs the ratio ϵ . The solid gray line represents the effective normalized plasma frequency of the system $\tilde{\omega}_p/\omega_p = (1 - i_b^2)^{1/4}$ resulting from the application of a bias current $i_b = 0.5$ (see Appendix B).

The frequency matching between ω_p^+ and the effective plasma frequency $\tilde{\omega}_p = \omega_p(1 - i_b^2)^{1/4}$ occurs at $\epsilon \simeq 0.7$ [see Fig. 3(b)], just close to the position of the minimum in the curves of τ_{MST} vs ϵ in Fig. 3(a). The resonant matching condition is robust enough to be observed with a different set of parameter values (see Appendix B). Furthermore, the position of this local minimum depends on both the coupling parameter γ and the applied bias current i_b , and moves towards lower values of ϵ for higher values of γ . For low values of i_b the resonant effect is more visible [Fig. 3(a)], while for higher bias values it tends to disappear as γ increases (see Appendix B). At low noise intensity, the resonant effect is still present, and even more evident (see Appendix B). Moreover, for $\epsilon \ll 1$ and $\epsilon \gg 1$, the curves approach two different plateaux. For $\epsilon \ll 1$, the two equations describing the dynamics of the two systems, JJ and axion, decouple,

since the effects of $\theta(t)$ on $\varphi(t)$ in Eq. (5a) are due to the term $(k_1/k_2)\epsilon \sin(\theta)$. For $\epsilon \gg 1$, the oscillations of $\theta(t)$ are highly damped, so as to compensate the high values of ϵ . This can be seen in Eq. (5b) where the term $(k_2/k_1)\epsilon \sin(\theta)$ is responsible for the sinusoidal shape of the potential felt by the axion. For $\epsilon \gg 1$ the potential well is extremely deep so that the axion oscillations are narrowly confined.

Furthermore, due to the term $(k_1/k_2)\epsilon \sin(\theta)$, which is always opposite to the bias term, the total effective current becomes smaller than i_b (results not shown). This feature indicates that the presence of an axion tends to confine the effective phase particle representing the JJ system behavior. This explains why the value of the MST tends to increase for $\epsilon \gtrsim 10^{-2}$. Thus, the two plateaux at low and high ϵ are somewhat different when $\gamma \gtrsim 0.5$, while for lower couplings the two plateaux are practically at the same level. In fact, for $\gamma \ll 1$ the weight of the term $(k_1/k_2)\epsilon \sin(\theta)$ is lessened by the presence of $k_1/k_2 = \gamma/(1 + \gamma)$, which vanishes if γ tends to zero and the axion-JJ equations decouple. Therefore, in the $\epsilon \gg 1$ region a MST that deviates significantly from the expected unperturbed value ($\epsilon \ll 1$) represents, together with the presence of the minimum, a *hallmark of an axion-JJ interaction* and therefore of the *axion detection*. The comparison between the MST measurements in the unperturbed case ($\epsilon \ll 1$), predicted also by Kramers theory, and those obtained for $\epsilon \gg 1$ can lead to an estimate of γ . In particular, first the behaviour of the MST as a function of the parameter ϵ is obtained. Afterwards, through a comparison of the theoretical curves shown in Figs. 3(a) and 4 with the experimental one, the value of the coupling parameter can be determined.

The observation that higher values of γ give higher values of the MST, both for $\epsilon \gg 1$ and for $\epsilon \ll 1$, is well justified too. In fact, since $(k_1/k_2)\epsilon \sin(\theta)$ effectively behaves as a current term in Eq. (5a), a stronger axion-JJ coupling results in an effective lower bias current which further confines the Josephson phase particle. This confinement, therefore, is due to both a greater axion-JJ coupling constant γ and a greater energy ratio ϵ .

This therefore identifies the suitable experimental conditions for a JJ-based axion detection. First, as the MST analysis is concerned, it has been shown that the underdamped regime is suitable to highlight the axion-induced effects on the JJ dynamics. Second, it has been found that for any value of the coupling parameter, according to the axion-mass estimates [31, 32], it is convenient to tune the plasma frequency, through the critical current, to reach the limit $\epsilon \gg 1$. This allows an improved estimate of the parameter γ , thanks to the greatest spacing between the curves related to different values of the axion-JJ coupling for $\gamma \gtrsim 0.5$. This makes the values of γ compatible with the experimental range of τ_{MST} more easily detectable for $\epsilon \gg 1$. Third, and most importantly, we have found a resonant activation phenomenon due to the frequency matching condition in the transition range $\epsilon \approx 1$.

The energy of the dark matter axion $m_a c^2$ is estimated in the energy range $\sim (0.006 - 2) \text{meV}$. To fulfill the $\varepsilon > 1$ condition requires a suitable JJ device with a sufficiently low critical current I_c , which can be even further reduced by heating and/or magnetic fields. Therefore, although the value of ε is not known precisely, it is still possible to design a setup to control its variation. This makes possible to range from the almost decoupled working regime ($\varepsilon \ll 1$) to the well coupled one ($\varepsilon > 1$).

VI. POSSIBLE EXPERIMENTAL SETUP

Based on the results previously shown, a technique to setup an experiment to detect the axion field is here outlined. First, as the parameter ε depends on the JJ critical current I_c , Eq. (6), by tuning I_c it is possible to measure the MST deviation from the dynamical regime characterized by high I_c (which entails small ε and for which the axion signal is ineffective) to that characterized by low I_c (which entails large ε and for which the axion signal is effective). Thus, as the critical current of the JJ is decreased, for instance by means of a magnetic field, the effects described by Eqs. (5) become more and more evident [see Fig. 3(a)] *in the same experimental set-up*. Finally, by tuning the frequency matching condition to observe the resonant phenomenon, the axion should be revealed.

Another possible experimental setup is to consider many JJs with significantly different critical currents and to observe an increase in the MSTs when the critical current passes the condition $\varepsilon \approx 1$, that is, after Eq.(6), $I_c \lesssim \frac{m_a^2 c^4}{\hbar 2e/C}$. Again, a tuning of the resonant matching condition should reveal the axion. We note that the increase in Fig. 3(a) is observed in normalized units; the relation between the actual (t_{MST}) and the normalized (τ_{MST}) average switching times also depends on the critical current: $t_{MST} = \tau_{MST} \frac{\hbar}{2eI_c R}$, according to the normalization of Eq. (A4). In other words, as ε increases due to the decrease in I_c , the amplification effect on the non-normalized MSTs should be even greater than that shown in Fig. 3(a).

VII. CONCLUSIONS

We have investigated the MSTs of a JJ directly coupled to an axion field and subject to both a dc bias current and thermal fluctuations. We have found the experimental conditions for a JJ-based axion detection: a) the underdamped regime; b) a Josephson plasma energy lower than the axion energy; c) the axion-induced resonant activation phenomenon, due to the occurrence of an effective frequency matching between axion and JJ, when the ratio of the axion energy to that of the junction falls

in the range $\varepsilon \in [0.1, 1]$. Furthermore, an experimental strategy for a JJ-based axion detection is proposed.

Perhaps most importantly, we propose to reveal the axion presence through the analysis of the escape times from the superconducting initial state. Thus, studying the switching time statistics, we have found a resonant activation phenomenon, based on the plasma frequency, induced on the JJ by the axion that turns out to act as an effective time-dependent oscillating bias current.

Finally, our approach can be applied to different physical scenarios, like damped pendula, two capacitively coupled JJs [57], excitable coupled JJs [58] and coupled qubits architectures for quantum computing [59, 60], paving the way to further theoretical achievements and new technological applications.

ACKNOWLEDGMENTS

Acknowledgments. This work was supported by Italian Ministry of University and Research (MIUR) and the Government of the Russian Federation through Agreement No. 074-02-2018-330 (2).

Appendix A

1. RCSJ Model

A short tunnel JJ is a quantum device formed by sandwiching a thin insulating layer between two superconducting electrodes, in which both lateral dimensions are smaller than the Josephson penetration depth [15]. The dynamics of the Josephson phase φ for a dissipative, current-biased short JJ can be studied within the RCSJ model [15, 18, 61] that in non-normalized units can be written as

$$\left(\frac{\Phi_0}{2\pi}\right)^2 C \frac{d^2\varphi}{dt^2} + \left(\frac{\Phi_0}{2\pi}\right)^2 \frac{1}{R} \frac{d\varphi}{dt} + \frac{d}{d\varphi} U = \left(\frac{\Phi_0}{2\pi}\right) I_N. \quad (\text{A1})$$

Here, U is the washboard potential along which the phase evolves,

$$U(\varphi, i_b) = E_{J_0} [1 - \cos(\varphi) - i_b \varphi], \quad (\text{A2})$$

where $E_{J_0} = (\Phi_0/2\pi) I_c$. The resulting activation energy barrier, $\Delta U(i_b)$, confines the phase φ in a metastable potential minimum and can be calculated as the difference between the maximum and minimum value of $U(\varphi, i_b)$. In units of E_{J_0} , it can be expressed as

$$\Delta \mathcal{U}(i_b) = \frac{\Delta U(i_b)}{E_{J_0}} = 2 \left[\sqrt{1 - i_b^2} - i_b \arccos(i_b) \right]. \quad (\text{A3})$$

In the phase particle picture, the term i_b represents the tilting of the potential profile; increasing i_b the slope of the washboard increases and the height $\Delta \mathcal{U}(i_b)$ of the

right potential barrier reduces, until this activation energy vanishes for $i_b = 1$, that is when the bias current reaches its critical value I_c .

If one normalizes the time to the inverse of the characteristic frequency, that is $\tau_c = \omega_c t$ with $\omega_c = (2e/\hbar) I_c R$, Eq. (A1) can be put in the dimensionless form

$$\beta_c \frac{d^2\varphi(\tau_c)}{d\tau_c^2} + \frac{d\varphi(\tau_c)}{d\tau_c} + \sin[\varphi(\tau_c)] = i_n(\tau_c) + i_b, \quad (\text{A4})$$

where $\beta_c = \omega_c RC$ is the Stewart-McCumber parameter. Usually, the single-harmonic current-phase relation (CPR) is appropriate to describe the features of a JJ [62], i.e., the high-order harmonic terms can be neglected. However, we observe that a non-sinusoidal CPR, as in the case of a short SNS junction [63], is not expected to undermine the feasibility of the Josephson-based scheme for axion detection discussed in this work, but only to slightly affect the specific switching time values. An overdamped junction has $\beta_c \ll 1$, that is a small capacitance and/or a small resistance. In contrast, a junction with $\beta_c \gg 1$ has a large capacitance and/or a large resistance, and is underdamped. Another way to obtain a dimensionless form of Eq. (A1) consists in normalizing with respect to the plasma frequency $\omega_p = \sqrt{2eI_c/\hbar C} \in [1, 1000]$ GHz. In this case the normalized RCSJ equation (A1) reads

$$\frac{d^2\varphi(\tau_p)}{d\tau_p^2} + \alpha \frac{d\varphi(\tau_p)}{d\tau_p} + \sin[\varphi(\tau_p)] = i_n(\tau_p) + i_b, \quad (\text{A5})$$

where $\alpha = 1/(\omega_p RC)$ is the damping parameter and $\tau_p = \omega_p t$. With this time normalization the under- and over-damped regimes correspond to $\alpha \ll 1$ and $\alpha \gg 1$, respectively.

We note that normalizing with respect to the characteristic frequency ω_c , as we did in our numerical simulations, the noise intensity D can be simply expressed as the ratio of thermal energy to Josephson coupling energy E_{J_0} , or $D = k_B T/E_{J_0}$, without any dependence on the damping. Normalizing instead with respect to the plasma frequency ω_p , the noise intensity becomes $D = \alpha k_B T/E_{J_0}$.

In our numerical simulations, for Gaussian fluctuations of amplitude D , the stochastic independent increment reads

$$\Delta i_N \simeq \sqrt{2D\Delta t} N(0, 1). \quad (\text{A6})$$

Here, the symbol $N(0, 1)$ indicates a random function Gaussianly distributed with zero mean and unit standard deviation. The stochastic integration of Eqs. (A4) or (A5) is performed with a finite-difference explicit method, using a time integration step $\Delta t = 10^{-2}$.

2. Axion parameters

An axion field a can be formally written as $a = f_a \theta$ [49, 64], where θ is the axion misalignment angle and f_a the

axion coupling constant. The axion's misalignment angle dynamics obeys the following homogeneous equation of motion [37]

$$\frac{d^2\theta(t)}{dt^2} + 3H \frac{d\theta(t)}{dt} + \frac{m_a^2 c^4}{\hbar^2} \sin[\theta(t)] = 0, \quad (\text{A7})$$

where m_a denotes the axion mass and $H \approx 2 \times 10^{-18} s^{-1}$ the Hubble parameter. The typical ranges of parameters that are allowed for dark matter axions are [65, 66]

$$3 \times 10^9 \text{ GeV} \leq f_a \leq 10^{12} \text{ GeV}. \quad (\text{A8})$$

and

$$6 \times 10^{-6} \text{ eV} \leq m_a c^2 \leq 2 \times 10^{-3} \text{ eV}. \quad (\text{A9})$$

The prediction of the axion's mass based on the average of the results obtained from five independent condensed matter experiments is [39–43]

$$m_a c^2 = (106 \pm 6) \mu\text{eV}. \quad (\text{A10})$$

These energies values permit to estimate the corresponding values of the energy ratio $\varepsilon = (m_a c^2/\hbar\omega_p)^2$, see Eq. (6). To do this, first of all the main parameters of Josephson must be set: for example, we can generically choose the values $R_a = 500 \Omega\mu\text{m}^2$, $C_s = 100 \text{ fF}/\mu\text{m}^2$, and $J_c = 10^6 \text{ A}/\text{m}^2$ for the resistance per area, the specific capacitance, and the critical current density, respectively, which gives a plasma frequency $\omega_p \simeq 170$ GHz and a Stewart-McCumber parameter $\beta_c \simeq 80$.

Then, from Eq. (A9) we get $\varepsilon \in (0.003 - 300)$, which is approximately the range of values we have explored in this work. Moreover, these values match the almost decoupled working regime ($\varepsilon \ll 1$) and the well coupled one ($\varepsilon > 1$), at which the τ_{MST} vs ε curves approach two different plateaux. Finally, the average value in Eq. (A10) corresponds to an energy ratio $\varepsilon \sim 0.85$, i.e., a value just close to the resonant matching condition discussed in Sec. V.

Appendix B: Linearization and Frequency Matching Condition

The interaction model proposed for a coupled axion-JJ system reads [Eqs. (4) of the main text]

$$\ddot{\varphi} + a_1 \dot{\varphi} + b_1 \sin(\varphi) = \gamma(\ddot{\theta} - \ddot{\varphi}), \quad (\text{B1a})$$

$$\ddot{\theta} + a_2 \dot{\theta} + b_2 \sin(\theta) = \gamma(\ddot{\varphi} - \ddot{\theta}), \quad (\text{B1b})$$

where γ is the coupling parameter. In the presence of both a bias and a stochastic current, by normalizing with respect to the squared plasma frequency $\omega_p^2 = b_1$, the system (4) can be rewritten as

$$\ddot{\varphi} + k_2 \alpha \dot{\varphi} + k_2 \sin(\varphi) + k_1 \varepsilon \sin(\theta) = k_2 [i_b + i_n], \quad (\text{B2a})$$

$$\ddot{\theta} + k_1 \alpha \dot{\theta} + k_1 \sin(\theta) + k_2 \varepsilon \sin(\varphi) = k_1 [i_b + i_n], \quad (\text{B2b})$$

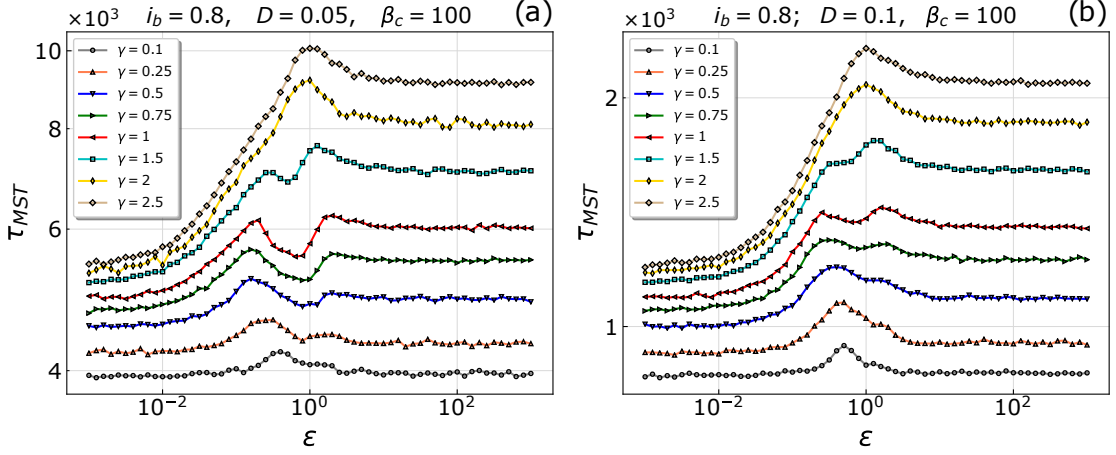


FIG. 4. Log-log plot of the dependence of the mean switching time τ_{MST} on the axion-JJ coupling ϵ , in underdamped regime ($\beta_c = 100$), with $i_b = 0.8$ and (a) $D = 0.05$, (b) $D = 0.1$ for a JJ subject to thermal noise and coupled with an axion field. The statistics is based on a set of $5 \cdot 10^4$ realizations.

with

$$\tau_p = \omega_p t, \quad \alpha = \frac{a_1}{\sqrt{b_1}} = \frac{1}{\omega_p RC} \approx 10^0 - 10^1, \quad (\text{B3a})$$

and the term proportional to $\dot{\theta}$ can be neglected, since

$$\frac{a_2}{\sqrt{b_1}} = \frac{3H}{\omega_p} \approx 10^{-30} \sim 0. \quad (\text{B4})$$

Normalizing with respect to the characteristic frequency ω_c , the system of differential equations becomes

$$\beta_c \ddot{\varphi} + k_2 \dot{\varphi} + k_2 \sin(\varphi) + k_1 \epsilon \sin(\theta) = k_2 [i_b + i_n], \quad (\text{B5a})$$

$$\beta_c \ddot{\theta} + k_1 \dot{\varphi} + k_1 \sin(\varphi) + k_2 \epsilon \sin(\theta) = k_1 [i_b + i_n], \quad (\text{B5b})$$

with $\tau_c = \omega_c t$.

In this work, by numerically solving Eqs. (5), we report the calculation of the MST as a function of the energy ratio ϵ . Specifically, in Fig. 4 the curves of MST versus ϵ are shown for a higher bias value, $i_b = 0.8$, with respect to that shown in Fig. 3(a) of the main text and for two noise intensity values, namely $D = 0.05$ and $D = 0.1$. These curves show that the resonant phenomenon tends to disappear for higher bias values and that it is still present and more evident at low noise intensity. Indeed, the resonant activation phenomenon is observed in the presence and in the absence of a noise source, see Refs. [16, 18, 56] (and references therein).

Let us consider the limit of small oscillations for both the JJ and the axion, in the absence of a noise source. In this case, we can approximate $\sin \varphi \sim \varphi$ and $\sin \theta \sim \theta$ in Eqs. (5). The resulting linearized system reads

$$\beta \ddot{\varphi} + \dot{\varphi} + \varphi + k\epsilon\theta = i_b, \quad (\text{B6a})$$

$$\beta \ddot{\theta} + k\dot{\varphi} + k\varphi + \epsilon\theta = ki_b, \quad (\text{B6b})$$

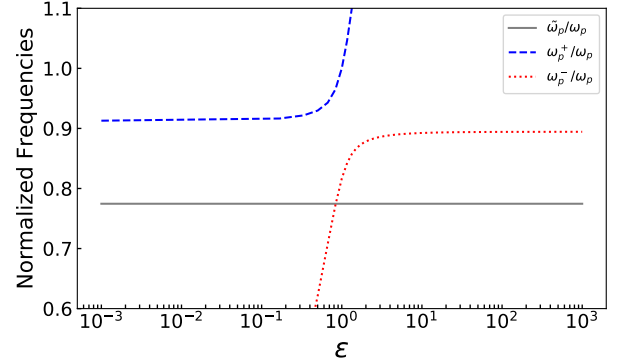


FIG. 5. Dependence of the two normalized frequencies $[\omega_p^+$ (dashed blue line) and ω_p^- (dotted red line)], which characterize the axion-JJ dynamics in the underdamped ($\beta_c = 100$) small-oscillation ($\dot{\varphi} \rightarrow 0$) regime, on the parameter ϵ , the ratio of the axion energy to the Josephson plasma energy, for the axion-JJ coupling $\gamma = 0.25$. The solid gray line represents the effective normalized plasma frequency of the system $\tilde{\omega}_p/\omega_p = (1 - i_b^2)^{1/4}$ resulting from the application of a bias current $i_b = 0.8$.

with $\beta = \beta_c/k_2$ and $k = k_1/k_2 = \gamma/1 + \gamma$. In the overdamped regime ($\beta_c \ll 1$), the first term can be neglected in both equations. By adding and subtracting the two equations, we obtain

$$\dot{\varphi} + \varphi - i_b = -\epsilon\theta, \quad (\text{B7a})$$

$$\dot{\varphi} + \varphi - i_b = \epsilon\theta, \quad (\text{B7b})$$

which implies

$$\dot{\varphi} + \varphi - i_b = 0 \quad \rightarrow \quad \varphi(\tau_c) = i_b + \frac{\varphi_0}{2} e^{-\tau_c}, \quad (\text{B8a})$$

$$\epsilon\theta = 0 \quad \rightarrow \quad \theta(\tau_c) = 0. \quad (\text{B8b})$$

Therefore, the two equations describing the dynamics of the two systems decouple. This indicates that the over-

damped linearized regime is unsuitable for axion detection.

In the underdamped regime the normalization with respect to ω_p allows to more easily interpret the frequency-matching phenomenon. Indeed, by putting $\alpha = 0$ (underdamped regime) in Eqs. (B2) and neglecting the noisy fluctuating current term, the linearized system, this time, remains coupled

$$\ddot{\varphi} + k_2\varphi + k_1\varepsilon\theta = k_2i_b, \quad (\text{B9a})$$

$$\ddot{\theta} + k_1\varphi + k_2\varepsilon\theta = k_1i_b. \quad (\text{B9b})$$

The analytical solutions, for the initial conditions considered in the main text, namely $[\varphi(0), \dot{\varphi}(0), \theta(0), \dot{\theta}(0)] = [\varphi_0, 0, 0, 0]$, are

$$\varphi(t) = i_b + (\varphi_0 - i_b) [A_-(\gamma, \varepsilon) \cos(\omega_p^+ t) + \varepsilon A_+(\gamma, \varepsilon) \cos(\omega_p^- t)], \quad (\text{B10a})$$

$$\theta(t) = (\varphi_0 - i_b) B(\gamma, \varepsilon) [\cos(\omega_p^+ t) + \cos(\omega_p^- t)] \quad (\text{B10b})$$

where

$$\omega_p^\pm(\gamma, \varepsilon) = \omega_p \sqrt{\frac{k_2(\varepsilon + 1) \pm f(\gamma, \varepsilon)}{2}}, \quad (\text{B11a})$$

$$f(\gamma, \varepsilon) = \sqrt{k_2^2(\varepsilon - 1)^2 + 4k_1^2\varepsilon}, \quad (\text{B11b})$$

$$A_\pm(\gamma, \varepsilon) = \frac{2K_1^2 + K_2 \pm K_2^2(\varepsilon - 1)}{1 + K_2(\varepsilon + 1)}, \quad (\text{B11c})$$

$$B(\gamma, \varepsilon) = K_1 = \frac{k_1}{f(\gamma, \varepsilon)}, \quad K_2 = \frac{k_2}{f(\gamma, \varepsilon)}. \quad (\text{B11d})$$

In Fig. 5 we show the behavior of the frequencies $\omega_p^\pm(\gamma, \varepsilon)$, in units of ω_p , as a function of ε at $\gamma = 0.25$ and $i_b = 0.8$. The black solid line indicates the bias-dependent plasma frequency $\tilde{\omega}_p/\omega_p = (1 - i_b^2)^{1/4}$. In Eq. (5), the term $k_1 \varepsilon \sin(\theta)$ can be considered as an *oscillating drive*, with two specific characteristic frequencies given by ω_p^\pm . Therefore, a resonant effect on the switching dynamics is expected when one of the two characteristic frequencies of the *oscillating drive* and the Josephson plasma frequency match. This is the resonant activation phenomenon observed both in the absence and in the presence of a noise source [16, 18]. In particular, in Fig. 5 it is shown the expected frequency matching at $\varepsilon \simeq 0.7$, that is just close to the position of the central minimum in the curves of τ_{MST} vs ε in Fig. 2 of the main text. Here, the frequency matching is with ω^- and the parameter values are different from those used to get the curves of Fig. 3 in the main text. This indicates that the resonant matching condition is robust enough to be observed with a different set of parameter values.

For $\varepsilon = 1$ we get the following simpler expressions

$$\varphi(\tau_p) = i_b + \frac{\varphi_0 - i_b}{2} \left[\cos(\tau_p) + \cos\left(\frac{\tau_p}{\sqrt{1 + 2\gamma}}\right) \right], \quad (\text{B12a})$$

$$\theta(\tau_p) = \frac{\varphi_0 - i_b}{2} \left[\cos(\tau_p) - \cos\left(\frac{\tau_p}{\sqrt{1 + 2\gamma}}\right) \right]. \quad (\text{B12b})$$

In this case, for small oscillations, the axion and the JJ are characterized by the same two frequencies: $\omega_1 = \omega_p$ and $\omega_2 = \omega_p/\sqrt{1 + 2\gamma}$, and the time evolutions of the two solutions appear very similar.

-
- [1] K. Nagano, H. Nakatsuka, S. Morisaki, T. Fujita, Y. Michimura, and I. Obata, Phys. Rev. D **104**, 062008 (2021).
- [2] A. Berlin, R. T. D’Agnolo, S. A. R. Ellis, and K. Zhou, Phys. Rev. D **104**, L111701 (2021).
- [3] D. Alesini, C. Braggio, G. Carugno, N. Crescini, D. D’Agostino, D. Di Gioacchino, R. Di Vora, P. Falferi, U. Gambardella, C. Gatti, et al., Phys. Rev. D **103**, 102004 (2021).
- [4] J.-W. Wang, X.-J. Bi, and P.-F. Yin, Phys. Rev. D **104**, 103015 (2021).
- [5] S. Chaudhuri, Journal of Cosmology and Astroparticle Physics **2021**, 033 (2021).
- [6] K. M. Backes, D. A. Palken, S. A. Kenany, B. M. Brubaker, S. B. Cahn, A. Droster, G. C. Hilton, S. Ghosh, H. Jackson, S. K. Lamoreaux, et al., Nature **590**, 238 (2021).
- [7] R. A. Battye, B. Garbrecht, J. I. McDonald, F. Pace, and S. Srinivasan, Phys. Rev. D **102**, 023504 (2020).
- [8] A. Arvanitaki, S. Dimopoulos, M. Galanis, L. Lehner, J. O. Thompson, and K. Van Tilburg, Phys. Rev. D **101**, 083014 (2020).
- [9] T. Braine, R. Cervantes, N. Crisosto, N. Du, S. Kimes, L. J. Rosenberg, G. Rybka, J. Yang, D. Bowring, A. S. Chou, et al. (ADMX Collaboration), Phys. Rev. Lett. **124**, 101303 (2020).
- [10] M. Buschmann, J. W. Foster, and B. R. Safdi, Phys. Rev. Lett. **124**, 161103 (2020).
- [11] K. Nagano, T. Fujita, Y. Michimura, and I. Obata, Phys. Rev. Lett. **123**, 111301 (2019).
- [12] M. Malnou, D. A. Palken, B. M. Brubaker, L. R. Vale, G. C. Hilton, and K. W. Lehnert, Phys. Rev. X **9**, 021023 (2019).
- [13] N. Du, N. Force, R. Khatiwada, E. Lentz, R. Ottens, L. J. Rosenberg, G. Rybka, G. Carosi, N. Woollett, D. Bowring, et al. (ADMX Collaboration), Phys. Rev. Lett. **120**, 151301 (2018).
- [14] B. M. Brubaker, L. Zhong, Y. V. Gurevich, S. B. Cahn, S. K. Lamoreaux, M. Simanovskaia, J. R. Root, S. M. Lewis, S. Al Kenany, K. M. Backes, et al., Phys. Rev. Lett. **118**, 061302 (2017).
- [15] A. Barone and G. Paterno, *Physics and applications of the Josephson effect* (Wiley, New York, 1982).
- [16] M. H. Devoret, J. M. Martinis, D. Esteve, and J. Clarke, Phys. Rev. Lett. **53**, 1260 (1984).
- [17] M. H. Devoret and R. J. Schoelkopf, Science **339**, 1169 (2013).
- [18] C. Guarcello, D. Valenti, and B. Spagnolo, Phys. Rev. B **92**, 174519 (2015).
- [19] F. S. Nogueira, Z. Nussinov, and J. van den Brink, Phys.

- Rev. Lett. **117**, 167002 (2016).
- [20] F. Tafuri, *Fundamentals and Frontiers of the Josephson Effect*, vol. 286 (Springer, Cham, Switzerland, 2019).
- [21] I. G. Irastorza and J. Redondo, *Progress in Particle and Nuclear Physics* **102**, 89 (2018).
- [22] A. I. Braginski, *Journal of Superconductivity and Novel Magnetism* **32**, 23 (2019).
- [23] M. Kjaergaard, M. E. Schwartz, J. Braumüller, P. Krantz, J. I.-J. Wang, S. Gustavsson, and W. D. Oliver, *Annual Review of Condensed Matter Physics* **11**, 369 (2020).
- [24] G.-H. Lee, D. K. Efetov, W. Jung, L. Ranzani, E. D. Walsh, T. A. Ohki, T. Taniguchi, K. Watanabe, P. Kim, D. Englund, et al., *Nature* **586**, 42 (2020).
- [25] E. D. Walsh, W. Jung, G.-H. Lee, D. K. Efetov, B.-I. Wu, K.-F. Huang, T. A. Ohki, T. Taniguchi, K. Watanabe, P. Kim, et al., *Science* **372**, 409 (2021).
- [26] A. Rettaroli, D. Alesini, D. Babusci, C. Barone, B. Buonomo, M. M. Beretta, G. Castellano, F. Chiarello, D. Di Gioacchino, G. Felici, et al., *Instruments* **5**, 022915 (2021).
- [27] C. Guarcello, D. Valenti, B. Spagnolo, V. Pierro, and G. Filatrella, *Nanotechnology* **28**, 134001 (2017).
- [28] A. V. Dixit, S. Chakram, K. He, A. Agrawal, R. K. Naik, D. I. Schuster, and A. Chou, *Phys. Rev. Lett.* **126**, 141302 (2021).
- [29] H. Murayama, in *Particle Physics and Cosmology: The Fabric of Spacetime*, edited by F. Bernardeau, C. Grojean, and J. Dalibard (Elsevier, 2007), vol. 86 of *Les Houches*, pp. 287–347.
- [30] R. Bradley, J. Clarke, D. Kinion, L. J. Rosenberg, K. van Bibber, S. Matsuki, M. Mück, and P. Sikivie, *Rev. Mod. Phys.* **75**, 777 (2003).
- [31] C. Beck, *Phys. Rev. Lett.* **111**, 231801 (2013).
- [32] C. Beck, *PoS EPS-HEP2017*, 058 (2017).
- [33] J. Yan and C. Beck, *Physica D: Nonlinear Phenomena* **403**, 132294 (2020).
- [34] C. Dessert, J. W. Foster, and B. R. Safdi, *The Astrophysical Journal* **904**, 42 (2020).
- [35] M. Malte Buschmann, R. T. Co, C. Dessert, and B. R. Safdi, *Physical Review Letters* **126**, 021102 (2021).
- [36] R. D. Peccei and H. R. Quinn, *Phys. Rev. Lett.* **38**, 1440 (1977).
- [37] R. T. Co, L. J. Hall, and K. Harigaya, *Phys. Rev. Lett.* **124**, 251802 (2020).
- [38] C.-F. Chang and Y. Cui, *Phys. Rev. D* **102**, 015003 (2020).
- [39] C. Hoffmann, F. Lefloch, M. Sanquer, and B. Pannetier, *Phys. Rev. B* **70**, 180503 (2004).
- [40] M.-H. Bae, R. C. Dinsmore III, M. Sahu, H.-J. Lee, and A. Bezryadin, *Phys. Rev. B* **77**, 144501 (2008).
- [41] L. He, J. Wang, and M. H. Chan, arXiv preprint arXiv:1107.0061 (2011).
- [42] T. E. Golikova, F. Hübner, D. Beckmann, I. E. Batov, T. Y. Karminskaya, M. Y. Kupriyanov, A. A. Golubov, and V. V. Ryazanov, *Phys. Rev. B* **86**, 064416 (2012).
- [43] L. Bretheau, Ç. Ö. Girit, H. Pothier, D. Esteve, and C. Urbina, *Nature* **499**, 312 (2013).
- [44] A. Piedjou Komnang, C. Guarcello, C. Barone, C. Gatti, S. Pagano, V. Pierro, A. Rettaroli, and G. Filatrella, *Chaos Solitons Fract* **142**, 110496 (2021), ISSN 0960-0779.
- [45] C. Guarcello, A. S. Piedjou Komnang, C. Barone, A. Rettaroli, C. Gatti, S. Pagano, and G. Filatrella, *Phys. Rev. Applied* **16**, 054015 (2021).
- [46] C. Guarcello, D. Valenti, B. Spagnolo, V. Pierro, and G. Filatrella, *Physical Review Applied* **11**, 044078 (2019).
- [47] C. Guarcello, G. Filatrella, B. Spagnolo, V. Pierro, and D. Valenti, *Physical Review Research* **2**, 043332 (2020).
- [48] C. Guarcello and F. Bergeret, *Phys. Rev. Applied* **13**, 034012 (2020).
- [49] P. Sikivie, *Phys. Rev. Lett.* **51**, 1415 (1983).
- [50] P. Dubos, H. Courtois, B. Pannetier, F. K. Wilhelm, A. D. Zaikin, and G. Schön, *Phys. Rev. B* **63**, 064502 (2001).
- [51] F. S. Bergeret and J. C. Cuevas, *Journal of Low Temperature Physics* **153**, 304 (2008).
- [52] X. Du, I. Skachko, and E. Y. Andrei, *Phys. Rev. B* **77**, 184507 (2008).
- [53] G. De Simoni, F. Paolucci, C. Puglia, and F. Giazotto, *ACS Nano* **13**, 7871 (2019).
- [54] R. Graham and T. Tél, *Phys. Rev. A* **31**, 1109 (1985).
- [55] R. L. Kautz, *Reports on Progress in Physics* **59**, 935 (1996).
- [56] C. R. Doering and J. C. Gadoua, *Phys. Rev. Lett.* **69**, 2318 (1992).
- [57] J. A. Blackburn, J. E. Marchese, M. Cirillo, and N. Grønbech-Jensen, *Physical Review B* **79**, 054516 (2009).
- [58] C. Hens, P. Pal, and S. K. Dana, *Physical Review E* **92**, 022915 (2015).
- [59] P. Krantz, M. Kjaergaard, F. Yan, T. P. Orlando, S. Gustavsson, and W. D. Oliver, *Applied Physics Reviews* **6**, 021318 (2019).
- [60] N. Grønbech-Jensen, J. E. Marchese, M. Cirillo, and J. A. Blackburn, *Phys. Rev. Lett.* **105**, 010501 (2010).
- [61] B. Spagnolo, C. Guarcello, L. Magazzù, A. Carollo, D. Persano Adorno, and D. Valenti, *Entropy* **19** (2017).
- [62] A. A. Golubov, M. Y. Kupriyanov, and E. Il'ichev, *Rev. Mod. Phys.* **76**, 411 (2004).
- [63] C. W. J. Beenakker, in *Low-Dimensional Electronic Systems*, edited by G. Bauer, F. Kuchar, and H. Heinrich (Springer Berlin Heidelberg, Berlin, Heidelberg, 1992), pp. 78–82.
- [64] L. Visinelli, *Modern Physics Letters A* **28**, 1350162 (2013).
- [65] P. Sikivie and Q. Yang, *Physical Review Letters* **103**, 111301 (2009).
- [66] L. D. Duffy and K. van Bibber, *New Journal of Physics* **11**, 105008 (2009).